Journal of Materials Chemistry

Cite this: J. Mater. Chem., 2012, 22, 25148

www.rsc.org/materials

PAPER

High-efficiency polymer photovoltaic cells using a solution-processable insulating interfacial nanolayer: the role of the insulating nanolayer

Kyung-Geun Lim,†[a] Mi-Ri Choi,†[a] Ho-Beom Kim,[a] Jong Hyeok Park[b] and Tae-Woo Lee*[a]

Received 27th July 2012, Accepted 1st October 2012
DOI: 10.1039/c2jm35016e

We employed a low-cost solution-processed ultrathin insulating polymeric layer of poly(4-hydroxystyrene) (PHS), with a high glass transition temperature ($T_g \sim 185$ °C), as an interfacial layer between the polymer:fullerene photoactive layer and the Al negative electrode for enhancing device power conversion efficiency (PCE) of polymer bulk-heterojunction photovoltaic cells and investigated the roles of the interfacial nanolayer by ultraviolet photoemission spectroscopy and capacitance–voltage measurement. The thin polymeric layer forms a dipole layer and causes the vacuum level of the adjacent negative electrode to shift upward, which resulted in an increase of the built-in potential. As a result, the open-circuit voltage and PCE of the device using a PHS nanolayer were remarkably improved. We finally achieved a very high PCE of 6.5% with the PHS/Al negative electrode which is even much better than that of the device using an Al electrode (5.0%). The solution-processed inexpensive PHS layer with a high T_g can be an attractive alternative to conventional vacuum-deposited low-work-function metal and insulating metal fluoride interfacial layers.

Introduction

Organic photovoltaic cells (OPVs) have been the focus of interest because of their potential for use as energy conversion devices.[1–9] The advantage of OPVs is that they can be more easily realized into flexible devices by low-cost and simple solution processes than inorganic solar cells. However, OPVs have practical limitations such as low power conversion efficiency (PCE), which is determined by open circuit voltage (V_{OC}), short circuit current (J_{SC}) and fill factor (FF). Achieving high PCE and long operational lifetime is one of the most crucial problems that must be solved before OPVs can be commercialized.

Most research to achieve high efficiency of OPVs has focused on the photoactive layers and control of their morphology.[2,3] To further improve the efficiency, it is quite necessary to develop interfacial layers between a photoactive layer and electrodes because the device performance of OPVs is largely dependent on the layers.[4–10] In the case of the ohmic contacts at both the electrodes in bulk-heterojunction OPVs, the highest occupied molecular orbital (HOMO) level of the donor polymer and the lowest unoccupied molecular orbital (LUMO) level of the acceptor are crucial factors for determining V_{OC}.[11] However, when the non-ohmic contact is formed in the conventional OPVs that have an indium-tin-oxide (ITO) positive electrode and an Al negative electrode, V_{OC} is determined by the work function difference between the two electrodes.[11] Therefore, modifying electrodes or introducing charge extraction layers has been used to improve V_{OC} and charge extraction of both the electrodes. Several different approaches such as incorporation of metal fluorides, TiOx, and low work function cathodes have been reported to improve the electron injection/extraction contact.[4–11] It is still a common method to insert a thin metal fluoride layer or low-work-function metal layer between the photoactive layer and the negative electrode by vacuum deposition. An approach introducing a thin polymeric layer by a solution process, instead of metal fluorides, is also promising to realize printable photovoltaic cells *via* a simple and low cost non-vacuum process.[12,13] Thin polymeric interfacial layers based on the conjugated polyelectrolyte have been used as a cathode interlayer in polymer light-emitting diodes and more recently OPVs. However, these ionic conjugated polymers have been synthesized *via* time-consuming long synthesis processes. Furthermore, polymers with a high glass transition temperature (T_g) are quite necessary to provide high thermal stability under hot outdoor operating conditions. Therefore, inexpensive insulating polar polymers having a high T_g prepared *via* a simple synthetic route are very useful as an interfacial layer for low-cost printable OPVs.

Here, we used a solution-processed ultrathin poly(4-hydroxystyrene) (PHS) layer (T_g: 183 °C) as an interfacial nanolayer (INL) between an polymer:fullerene photoactive layer and an Al electrode. The alcohol-soluble PHS enables orthogonal film processing on a polymeric active layer without dissolving the

[a]*Dept. of Materials Science and Engineering, Pohang University of Science and Technology (POSTECH), San 31 Hyoja-dong, Nam-gu, Pohang, Gyeongbuk 790-784, Korea. E-mail: twlee@postech.ac.kr; Fax: +82-54-279-2399; Tel: +82-54-279-2151*
[b]*School of Chemical Engineering and SKKU Advanced Institute of Nanotechnology (SAINT), Sungkyunkwan University, Suwon 440-746, Korea*
† These authors contributed equally to this study.

underneath layer. We also investigated the roles of an INL in bulk-heterojunction OPVs, by analyzing the influence of INLs on electronic states. The PHS nano-layer on a photoactive layer induces a dipole layer whose direction is toward the active layer. We found that due to the vacuum level shift at the negative electrode, the built-in voltage and V_{OC} of the device increased, which was evidenced by ultraviolet photoelectron spectroscopy and capacitance–voltage measurement. As a result, PCE was remarkably improved. We achieved a very high PCE value of the OPV with a PHS layer (6.5%) which was much higher than that of the OPV without using the PHS layer (5.0%) as well. These results demonstrate the feasibility of using a solution-processed PHS layer to replace the vacuum-deposited metal fluoride or the low-work-function metal layer.

Results and discussion

We used an ultrathin polymeric PHS layer as an INL in solution processed OPVs and its chemical structure is shown in Fig. 1. We used two different polymer–fullerene blends as a photoactive layer, which is composed of regioregular poly(3-hexylthiophene) (P3HT) and [6,6]-phenyl C60-butyric acid methyl ester (PCBM) or poly(*N*-9′-hepta-decanyl-2,7-carbazole-*alt*-5,5-(4′,7′-di-2-thienyl-2′,1′,3′-benzothiadiazole) (PCDTBT):[6,6]-phenyl C70-butyric acid methyl ester ($PC_{70}BM$). We utilized poly(3,4-ethylenedioxythiophene):poly(4-styrenesulfonate) (PEDOT:PSS) (Baytron PH, work function: ~4.9 eV) as a hole extraction layer for P3HT:PCBM devices and the PEDOT:PSS/perfluorinated ionomer (PHPF161) (work function: ~5.4 eV)[14] for PCDTBT:$PC_{70}BM$. Fig. 1 depicts our structure of the OPVs (ITO/PEDOT:PSS/P3HT:PCBM/INL/Al and ITO/PHPF161/PCDTBT:$PC_{70}BM$/INL/Al). To demonstrate the effect of the PHS INL, we compared them to devices that did not include an INL, and to devices that included a conventional thin LiF or Ca layer deposited under high vacuum (<5 × 10^{-7} Torr). A PHS solution with a very low concentration in ethyl alcohol was deposited on a photo-active layer by spin-coating to form a nano-scale interfacial layer. We measured the thicknesses of thin PHS layers on a Si wafer using the ellipsometry. The actual thickness of a photo-active layer may be a little different because of different surface energy and morphology of the photoactive layer from those of the Si wafer. We optimized the thickness of the PHS layer (2.7 nm on a Si wafer) in order to maximize the effect of an interfacial layer.

We observed current density–voltage (J–V) characteristics of OPV devices with an ultrathin PHS INL (2.2–5.5 nm) and compared with those of the devices without an INL and the devices with a LiF or Ca layer, as shown in Fig. 2. Fig. 2a and c show the J–V curves of P3HT:PCBM and PCDTBT:$PC_{70}BM$

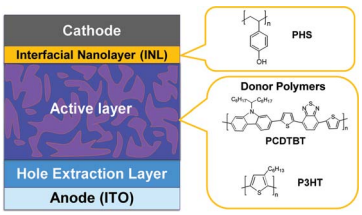

Fig. 1 Structure of organic photovoltaic cells using PHS as an interfacial nanolayer (INL).

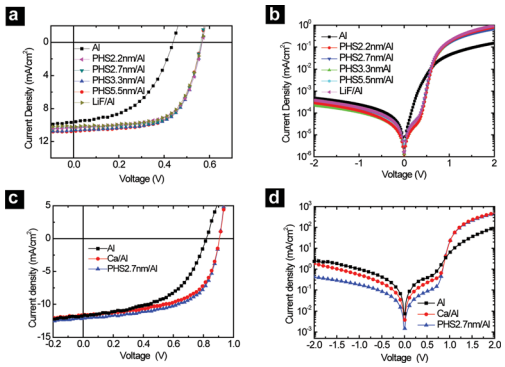

Fig. 2 The current density–voltage (J–V) curves of P3HT:PCBM (a and b) and PCDTBT:$PC_{70}BM$ (c and d) devices with and without interfacial nanolayers under AM 1.5 illumination at an irradiation intensity of 100 mW cm^{-2} (a and c) and under dark conditions (b and d).

devices under continuous solar simulated air-mass 1.5 global (AM 1.5 G) irradiation at 100 mW cm^{-2}, respectively, and Fig. 2b and d show the results under dark conditions. Table 1 summarizes the device characteristics in terms of J_{SC}, V_{OC}, FF and PCE with different INLs. The V_{OC} values of the devices using a PHS INL were remarkably improved compared with the reference device without using any INL. The FF values also increased in the devices with a PHS layer compared with those of the reference device. As a result, PCEs of the devices with a PHS layer (2.2–3.3 nm) were 3.9% for P3HT:PCBM and 6.5% for PCDTBT:$PC_{70}BM$ which were much higher than those of the reference devices (2.1 and 5.0%). It is noted that the PCEs of PCDTBT devices using a PHS layer are higher than even that of a device using a thin Ca (3 nm) layer. The improvement of V_{OC} can be attributed to the increase of the built-in-potential of the devices with a PHS layer resulting from the upward shift of the vacuum level at the negative electrode. The J_{SC} values were almost the same, irrespective of the use of the interfacial layers, even if we observed a large current increase due to facilitated electron injection by a PHS INL in the device under dark conditions (Fig. 2b and d).[15] The devices including a PHS INL (2.7 nm) achieved a higher shunt resistance (R_{sh}) and a lower series resistance (R_s) than those of the devices without an INL; R_{sh} = 782.4 (P3HT) and 555.6 ohm cm^2 (PCDTBT), R_s = 7.16 (P3HT) and 6.8 ohm cm^2 (PCDTBT) for the device with a PHS INL and R_{sh} = 196.8 (P3HT) and 366.0 ohm cm^2 (PCDTBT), R_s = 10.6 (P3HT) and 16.4 ohm cm^2 (PCDTBT) for the devices without an INL. They led to the increased FF of the PHS device from 49.7 to 63.7 % for P3HT:PCBM and from 51.9 to 59.1 % for PCDTBT:$PC_{70}BM$.[16]

The increase in V_{OC} in the device that includes a PHS INL can be attributed to a dipole layer which is induced by a thin PHS layer. Fig. 3 shows the schematic energy level of the OPVs; Fig. 3a is for the reference OPV and Fig. 3b is for the OPV using a PHS INL. On the hydrophobic surface of an active layer, the backbone of the PHS layer, which has relatively hydrophobic property, tends to face toward an active layer. The negatively charged parts (*e.g.*, hydroxyl groups) are naturally arranged in the opposite direction. As a result, at the interface between the active layer and the negative electrode, the dipole layer points away from the negative electrode as described in Fig. 3b(I).

Table 1 Performance measurement of polymer photovoltaic cells

Photoactive layer	INL[a]	V_{OC} [V]	J_{SC} [mA cm^{-2}]	FF [%]	PCE [%]
P3HT:PCBM	—	0.43	9.7	49.7	2.1[b] (2.03 ± 0.05)[c]
P3HT:PCBM	LiF	0.56	10.2	64.9	3.7 (3.57 ± 0.07)
P3HT:PCBM	PHS2.2 nm	0.56	10.8	64.3	3.9 (3.83 ± 0.06)
P3HT:PCBM	PHS2.7 nm	0.57	10.7	63.7	3.9 (3.80 ± 0.08)
P3HT:PCBM	PHS3.3 nm	0.56	10.4	66.6	3.9 (3.85 ± 0.05)
P3HT:PCBM	PHS5.5 nm	0.57	10.3	63.2	3.7 (3.63 ± 0.05)
PCDTBT:$PC_{70}BM$	—	0.82	11.7	51.9	5.0 (4.84 ± 0.20)
PCDTBT:$PC_{70}BM$	Ca	0.90	11.6	58.3	6.1 (6.07 ± 0.02)
PCDTBT:$PC_{70}BM$	PHS2.7 nm	0.90	12.1	59.1	6.5 (6.45 ± 0.03)

[a] Interfacial nanolayer (INL) between an active layer and a cathode. [b] The maximum PCE. [c] The average value of PCE ± standard deviation of four devices.

Many studies have investigated the change of the electronic energy levels due to the presence of the molecular dipoles. The dipole layers have been used to adjust the work function and to increase the efficiency of charge injection/extraction.[16–21] Like other cases, the dipole layer of PHS makes relatively the upward shift of the vacuum level of the adjacent negative electrode layer. The difference of effective work functions between two electrodes can be enlarged due to this vacuum level shift. Fig. 3(II) and (III) depict energy level alignment of OPV devices under short circuit (*i.e.* no electric field) and open-circuit (*i.e.* flat band) conditions, respectively. The Fermi levels of metal electrodes in metal–semiconductor–metal structures are aligned at equilibrium under short circuit conditions (Fig. 3a(II)). In the case of the device with the PHS INL, the bending of conduction and valence bands becomes much steeper than that of the reference device without the INL because of the upward shift of the vacuum level of the negative electrode, implying the decrease of the effective work function of the negative electrode. Furthermore, the larger difference in the effective work function between two electrodes caused a larger built-in voltage. In other words, the built-in voltage (Δ) that is required to make flat band conditions increased upon adding the PHS layer ($\Delta_2 > \Delta_1$). Consequently, the V_{OC} of the device with a PHS layer was remarkably improved because the V_{OC} tends to increase with the increasing built-in voltages in these bulk-heterojunction OPVs.

Jönsson *et al.* reported the role of LiF between a negative electrode and an active layer in polymer solar cells.[22] According to the reaction model, the thermally deposited LiF tends to decompose upon deposition of reactive Al on LiF and then release Li to make a low work function contact.[22]

Due to the large dipole moment of LiF (6.33 D) to decrease the surface potential of the Al, the lowered effective work function of the negative electrode can also be understood based on the dipole model.[23] The fact that the OPV device with a PHS layer showed almost identical device characteristics to the device with a LiF layer implies that the mechanism of the PHS INL in OPVs is analogous to the dipole model of the LiF layer because there is no chemical reaction between the photoactive layer and the PHS INL.

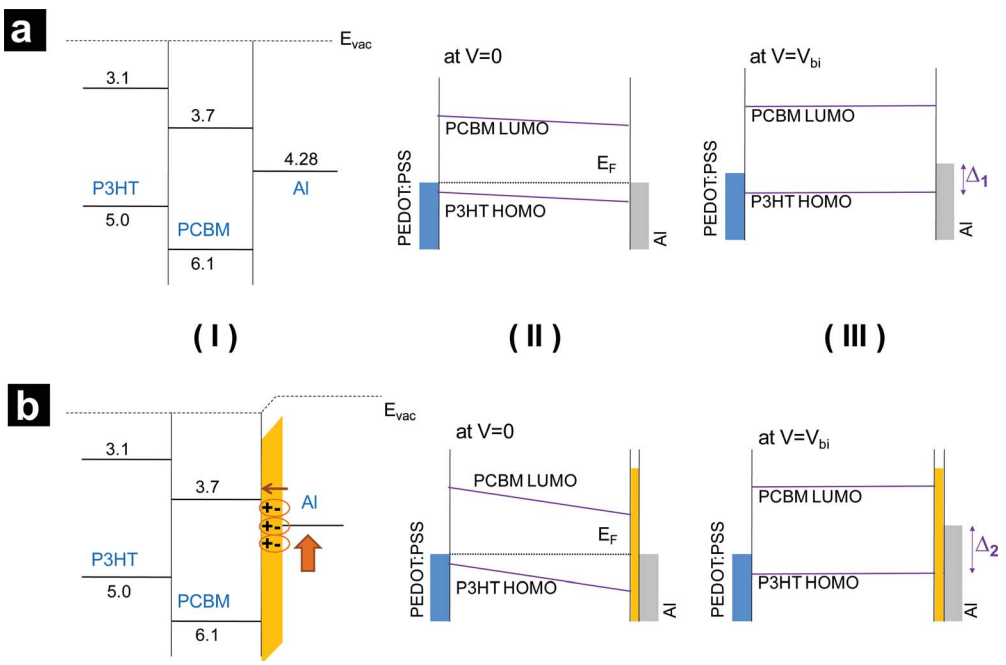

Fig. 3 The schematic energy diagram of solar cells depending on the applied bias. Device structure: (a) ITO/PEDOT:PSS/P3HT:PCBM/Al and (b) ITO/PEDOT:PSS/P3HT:PCBM/PHS/Al. The vacuum level shift and energy levels are depicted in the schematic energy diagram (I). The energy band bending is also depicted under short-circuit conditions (II) and open circuit conditions (flat band conditions) (III).

We investigated the electronic and energetic structures of photoactive surface layers with or without a PHS layer using ultraviolet photoelectron spectroscopy (UPS). We prepared two samples on Si wafers in the same way as the devices were fabricated: one had only a P3HT:PCBM active layer on the Si wafer, and the other had a very thin PHS layer on the active layer. Fig. 4 shows the secondary cutoff of UPS spectra of two samples. The change between the UPS spectra of the two samples appeared only at the secondary electron cutoff on the high binding energy side, as shown in Fig. 4. If the PHS layer is deposited on an active layer, the secondary cutoff of a P3HT:PCBM layer under the thin PHS layer shifts leftward by 0.43 eV, compared with that of only P3HT:PCBM layer. This shift is related to the reduction in the vacuum level of the P3HT:PCBM layer with a PHS layer as depicted in the schematic energy diagram of Fig. 3b.

To better understand the effects of the PHS INL, we analyzed the capacitance–voltage (C–V) characteristics at 1000 Hz (Fig. 5) using the P3HT:PCBM devices described in Fig. 1 and 2. The OPVs with two different INLs (LiF and PHS 2.7 nm) have quite different capacitance–voltage behaviors from the device without an INL (Fig. 5). As the bias voltage increased, the capacitances of devices increased up to each peak and then decreased. The device without an INL showed a distinct peak at 0.38 V in the capacitance–voltage curve. The devices that include a LiF or PHS INL showed much higher distinct peak capacitance at 0.54 and 0.54 V, respectively. We call the voltage with the peak capacitance as the peak voltage (V_{peak}) which is correlated with the built-in voltage (V_{bi}) according to the following relationship.[24]

$$V_{bi} - V_{peak} \propto \frac{k_B T}{e} \quad (1)$$

where k_B is the Boltzmann constant and T is the temperature. Similar to the V_{OC} in OPVs, the V_{peak} is always smaller than V_{bi} at room temperature due to the space charges near the electrodes and becomes closer to the V_{bi} as the temperature decreases. Therefore, at room temperature, the V_{peak} is considered as an effective value of the V_{bi}. The higher V_{peak} with INLs indicates the higher V_{bi} in OPVs.

The capacitance is mainly correlated with the accumulated space charges inside the devices. It implies that the V_{peak} is observed when the device is under open circuit conditions (or flat band conditions). Above the open circuit voltage, the capacitance tends to decrease sharply due to recombination of the space charges with injected opposite charges. As described above, the bending of conduction and valence bands becomes much steeper

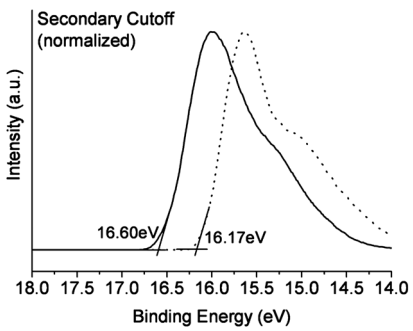

Fig. 4 UPS spectra of the P3HT:PCBM layer (dotted line) and P3HT:PCBM layer with a PHS interfacial layer (solid line).

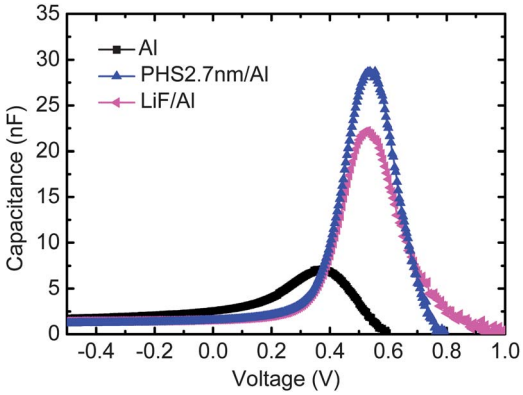

Fig. 5 Effects of an interfacial nanolayer on capacitance–voltage (C–V) curves of P3HT:PCBM devices at 1000 Hz.

in the device with INL than without the INL (Fig. 3a(II) and b(II)), therefore the applied voltage required for open circuit conditions (or flat band conditions) is much larger in the device with INL (Fig. 3a(III) and b(III)). The V_{peak} with a PHS INL (0.54 V) is the same as that with a LiF INL (0.54 V), which also indicates that the PHS and LiF INLs had a quite similar effect on the improvement of V_{bi} and thus V_{OC}.

Conclusions

We used an inexpensive solution-processable polar polymer with a high T_g, PHS, as an INL to improve PCE in bulk-heterojunction OPVs and elucidated the working mechanism of the INL. Our UPS and capacitance–voltage measurements revealed that the PHS nano-layer on a photoactive layer induces a dipole layer whose direction is toward the active layer, which causes the upward vacuum level shift at the negative electrode and thus remarkable increase of the built-in voltage and V_{OC}. As a result, PCE was remarkably improved. Finally, we achieved a very high PCE value (6.5%) in the PCDTBT:PC_{70}BM device using the PHS INL which is much higher than that in the device without using the PHS layer (5.0%). Using the inexpensive PHS INL also has the advantages that it can be deposited using a simple and inexpensive solution process that does not require high-vacuum conditions. Our results strongly indicate that the inexpensive PHS INL with a high T_g can be a promising candidate to replace a conventional LiF and Ca interfacial layer in low-cost, printed OPVs.

Experimental

Organic photovoltaic cell fabrication

On the top of cleaned indium-tin-oxide (ITO)/glass, the PEDOT:PSS (CLEVIOS™ PH) diluted in isopropyl alcohol with a 1 : 1 volume ratio was spin-coated in 35 nm thickness as the hole extraction layer, followed by baking on a hotplate in air at 200 °C for 10 min. The active layer which is composed of a 1 : 1 mixture of poly(3-hexylthiophene) (P3HT) (regioregularity > 98%, average weight average molecular weight (M_w) ~25 700) from Rieke Metals Inc.) and [6,6]-phenyl C60-butyric acid methyl ester (PCBM) (from nano-C Inc.) in 1,2-dichlorebenzene was spin coated to make 210 nm thick films on the PEDOT:PSS layer and then baked in a vacuum hotplate at 150 °C for 30 min

and cooled for 10 min. Another blend of PCDTBT (1-material) (7 mg) and $PC_{70}BM$ (Nano-c) (28 mg) in 1 ml DCB was also prepared for the photoactive layer. PCDTBT:$PC_{70}BM$ layers were spin-coated at 1600 rpm for 60 s to make 80 nm thick films and then thermally annealed at 70 °C for 10 min in the N_2 glove box. For the device using a PHS layer as an INL, a PHS solution dissolved in ethyl alcohol was deposited by spin-coating and then dried at 50 °C for 10 min. The thickness of the INL was controlled by solution concentration and spin coating conditions. The average thickness and standard deviation were measured by ellipsometry as 2.24 ± 0.7 nm at 5000 rpm with 0.08 wt% solution, 2.74 ± 0.6 nm at 1000 rpm with 0.08 wt% solution, 3.38 ± 0.7 nm at 1500 rpm with 0.12 wt% solution, and 5.54 ± 0.2 nm at 5500 rpm with 0.12 wt% solution. We performed UPS measurement by using the He I (21.22 eV) photon lines of a He-discharge lamp at 4B1, Pohang Accelerator Laboratory, Korea. The total energy resolution of the UPS measurement was 50 meV and we compared it with the INL on top of the P3HT:PCBM layer and the bare P3HT:PCBM layer without the INL. The dipole of the INL is defined here as the vacuum level shift, determined at a different position of the secondary cutoff. For the device using a LiF layer as an INL, a 1 nm thick LiF layer was deposited under high vacuum ($<5 \times 10^{-7}$ Torr). Then, the 100 nm thick Al was deposited either on the P3HT:PCBM and PCDTBT:$PC_{70}BM$ photoactive layers (reference devices) or on the INL (PHS or LiF)/the photoactive layers (PHS device and LiF device) under high vacuum below 5×10^{-7} Torr. The devices were encapsulated with a glass lid using a UV-curable epoxy resin.

Device characterization

Current–voltage (*J–V*) characteristics were recorded by using a computer-controlled Keithley 2400 Source Meter under simulated AM 1.5 G irradiation at 100 mW cm^{-2} generated using a Xenon lamp-based solar simulator system (Newport 94043A, Class AAA, 450 W). The light intensity was calibrated *versus* a reference solar cell (Newport 91150V). All pixels were 6 mm^2 and all measurements were conducted in air at room temperature.

The capacitance–voltage (*C–V*) measurements of the devices were conducted at the room temperature in the dark, using Neoscience Biologic SP-300. The devices were biased from −1 V to + 1 V and superimposed with AC drive voltage with a constant frequency of 1000 Hz.

Acknowledgements

This research was supported by the Basic Research Program through the National Research Foundation of Korea (NRF), funded by the Ministry of Education, Science and Technology (no. 2010-0026281). This work was also supported by a grant (Code no. 2011-0031639) from the Center for Advanced Soft Electronics under the Global Frontier Research Program of the Ministry of Education, Science and Technology, Korea.

References

1 G. Dennler, M. C. Scharber and C. J. Brabec, *Adv. Mater.*, 2009, **21**, 1323; C. J. Brabec, S. Gowrisanker, J. J. M. Halls, D. Laird, S. Jia and S. P. Williams, *Adv. Mater.*, 2010, **22**, 3839; M. Helgesen, R. Søndergaard and F. C. Krebs, *J. Mater. Chem.*, 2010, **20**, 36; J. Peet, A. J. Heeger and G. C. Bazna, *Acc. Chem. Res.*, 2009, **42**, 1700–1708; J. Peet, M. L. Senatore, A. J. Heeger and G. C. Bazan, *Adv. Mater.*, 2009, **21**, 1521–1527; H. B. Yang, Q. L. Song, C. M. Li and Z. S. Lu, *Energy Environ. Sci.*, 2008, **1**, 389; T. Ameri, G. Dennler, C. Lungenschmied and C. J. Brabec, *Energy Environ. Sci.*, 2009, **2**, 347; M. K. Siddiki, J. Li, D. Galipeau and Q. Qiao, *Energy Environ. Sci.*, 2010, **3**, 867.

2 H.-Y. Chen, J. Hou, S. Zhang, Y. Liang, G. Yang, Y. Yang, L. Yu, Y. Wu and G. Li, *Nat. Photonics*, 2009, **3**, 649; S. H. Park, A. Roy, S. Beaupre, S. Cho, N. Coates, J. S. Moon, D. Moses, M. Leclerc, K. Lee and A. J. Heeger, *Nat. Photonics*, 2009, **3**, 297; W. Ma, C. Yang, X. Gong, K. Lee and A. J. Heeger, *Adv. Funct. Mater.*, 2005, **15**, 1617; P. Schilinsky, U. Asawapirom, U. Scherf, M. Biele and C. J. Brabec, *Chem. Mater.*, 2005, **17**, 2175; C. Yang, J. G. Hu and A. J. Heeger, *J. Am. Chem. Soc.*, 2006, **128**, 12007; G. Li, V. Shrotriya, J. Huang, Y. Yao, T. Moriarty, K. Emery and Y. Yang, *Nat. Mater.*, 2005, **4**, 864; J. Xue, B. P. Rand, S. Uchida and S. R. Forrest, *J. Appl. Phys.*, 2005, **98**, 124903; R. J. Kline, M. D. Mcgehee and M. F. Toney, *Nat. Mater.*, 2006, **5**, 222; X. Yang, J. Loos, S. C. Veenstra, W. J. H. Verhees, M. M. Wienk, J. M. Kroon, M. A. J. Michels and R. A. J. Janssen, *Nano Lett.*, 2005, **5**, 579.

3 F. Zhang, W. Mammo, L. M. Andersson, S. Admassie, M. R. Andersson and O. Inganas, *Adv. Mater.*, 2006, **18**, 2169; W.-Y. Wong, X.-Z. Wang, Z. He, A. B. Djurisic, C.-T. Yip, K.-Y. Cheung, H. Wang, C. S. K. Mak and W.-K. Chan, *Nat. Mater.*, 2007, **6**, 521; M. Morana, M. Wegscheider, A. Bonanni, N. Kopidakis, S. Shaheen, M. Scharber, Z. Zhu, D. Waller, R. Gaudiana and C. J. Brabec, *Adv. Funct. Mater.*, 2008, **18**, 1757; J. Gilot, M. M. Wienk and R. A. J. Janssen, *Nat. Mater.*, 2007, **6**, 704; T. Erb, U. Zhokhavets, G. Gobsch, S. Raleva, B. Stühn, P. Schilinsky, C. Waldauf and C. J. Brabec, *Adv. Funct. Mater.*, 2005, **15**, 1193; M. H. Yun, G.-H. Kim, C. Yang and J. Y. Kim, *J. Mater. Chem.*, 2010, **20**, 7710.

4 R. Steim, F. R. Koglera and C. J. Brabec, *J. Mater. Chem.*, 2010, **20**, 2499.

5 T.-W. Lee, K.-G. Lim and D.-H. Kim, *Electron. Mater. Lett.*, 2010, **6**, 41.

6 J. H. Park, T.-W. Lee, B.-D. Chin, D. H. Wang and O. O. Park, *Macromol. Rapid Commun.*, 2010, **31**, 2095.

7 J. Y. Kim, S. H. Kim, H.-H. Lee, K. Lee, W. Ma, X. Gong and A. J. Heeger, *Adv. Mater.*, 2006, **18**, 572; S.-H. Lee, J.-H. Kim, T.-H. Shim and J.-G. Park, *Electron. Mater. Lett.*, 2008, **4**, 19; H. Choi, H. Cho, S. Song, H. Suh, S. Park and J. Y. Kim, *Phys. Chem. Chem. Phys.*, 2010, **12**, 15309; B. R. Lee, H. Choi, J. S. Park, H. J. Lee, S. O. Kim, J. Y. Kim and M. H. Song, *J. Mater. Chem.*, 2011, **21**, 2051.

8 X. Jiang, H. Xu, L. Yang, M. Shi, M. Wang and H. Chen, *Sol. Energy Mater. Sol. Cells*, 2009, **93**, 650.

9 M. O. Reese, M. S. White, G. Rumbles, D. S. Ginley and S. E. Shaheen, *Appl. Phys. Lett.*, 2008, **92**, 053307.

10 J. H. Park, O. O. Park, J. W. Yu, J. K. Kim and Y. C. Kim, *Appl. Phys. Lett.*, 2004, **84**, 1783; T.-W. Lee, M. G. Kim, S. H. Park, S. Y. Kim, O. Kwon, T. Noh, J.-J. Park, T.-L. Choi, J. H. Park and B. D. Chin, *Adv. Funct. Mater.*, 2009, **19**, 1863.

11 V. D. Mihailetchi, P. W. M. Blom, J. C. Hummelen and M. T. Rispens, *J. Appl. Phys.*, 2003, **94**, 6849.

12 F. Zhang, M. Ceder and O. Inganäs, *Adv. Mater.*, 2007, **19**, 1835.

13 S. -I. Na, S. -H. Oh, S. -S. Kim and D. -Y. Kim, *Org. Electron.*, 2009, **10**, 496.

14 T.-H. Han, Y. Lee, M.-R. Choi, S.-H. Woo, S.-H. Bae, B. H. Hong, J.-H. Ahn and T.-W. Lee, *Nat. Photonics*, 2012, **6**, 105; T.-W. Lee, Y. Chung, O. Kwon and J.-J. Park, *Adv. Funct. Mater.*, 2007, **17**, 390; T.-W. Lee, O. Kwon, M.-G. Kim, S. H. Park, J. Chung, S. Y. Kim, Y. Chung, J.-Y. Park, E. Han, D. H. Huh, J.-J. Park and L. Pu, *Appl. Phys. Lett.*, 2005, **87**, 231106.

15 This can be attributed to the different current pathway of electron extraction at the negative electrode interface from electron injection. Under short-circuit conditions, the electrons can be extracted dominantly through the LUMO level of the PCBM where the negative electrodes are pinned to. However, above the open-circuit voltage, the electron injection can take place into the P3HT as well as PCBM, resulting in a large increase of dark current in the devices with an INL such as LiF and PHS.

16 H.-L. Yip, S. K. Hau, N. S. Baek and A. K.-Y. Jen, *Appl. Phys. Lett.*, 2008, **92**, 193313.
17 B. de Boer, A. Hadipour, M. M. Mandoc, T. van Woudenbergh and P. W. M. Blom, *Adv. Mater.*, 2005, **17**, 621.
18 H. L. Yip, S. K. Hau, N. S. Baek, H. Ma and A. K. Y. Jen, *Adv. Mater.*, 2008, **20**, 2376.
19 X. Crispin, V. Geskin, A. Crispin, J. Cornil, R. Lazzaroni, W. R. Salaneck and J.-L. Brédas, *J. Am. Chem. Soc.*, 2002, **124**, 8131.
20 C. Goh, S. R. Scully and M. D. McGehee, *J. Appl. Phys.*, 2007, **101**, 114503.
21 W. Osikowicz, M. P. de Jong and W. R. Salaneck, *Adv. Mater.*, 2007, **19**, 4213.
22 S. K. M. Jönsson, E. Carlegrim, F. Zhang, W. R. Salaneck and M. Fahlman, *Jpn. J. Appl. Phys.*, 2005, **44**, 3695.
23 S. E. Shaheen, G. E. Jabbour, M. M. Morrell, Y. Kawabe, B. Kippelen, N. Peyghambarian, M.-F. Nabor, R. Schlaf, E. A. Mash and N. R. Armstrong, *J. Appl. Phys.*, 1998, **84**, 2324.
24 S. L. M. van Mensfoort and R. Coehoorn, *Phys. Rev. Lett.*, 2008, **100**, 086802.